

Journal Name

ARTICLE TYPE

Cite this: DOI: 00.0000/xxxxxxxxxx

Received Date

Accepted Date

DOI: 00.0000/xxxxxxxxxx

Faster grain-boundary diffusion with a higher activation enthalpy than bulk diffusion in ionic space-charge layers

Timon F. Kielgas,^a Roger A. De Souza^{*a}

Faster diffusion of cations along grain boundaries is reported in the literature for a variety of acceptor-doped ABO_3 perovskite-type oxides. The ratio r of the activation enthalpy of grain-boundary diffusion (ΔH^{gb}) to the activation enthalpy of bulk diffusion (ΔH^b) is seen experimentally to lie in the range $0.7 < r = \Delta H^{gb}/\Delta H^b < 1.3$, albeit with substantial errors. In a previous publication [Parras and De Souza, *Acta Mater.* 195 (2020) 383] it was shown through a set of continuum simulations that cation-vacancy accumulation within negative space-charge layers at grain boundaries in acceptor-doped perovskites will give rise to faster grain-boundary diffusion of cations, with the associated values of r approaching but not exceeding unity. In the present study, we demonstrate by means of continuum simulations that under certain conditions $r > 1$ is achievable for faster cation diffusion along grain boundaries in an acceptor-doped perovskite ceramic. Diffusion profiles for a two-dimensional bicrystal geometry are obtained by solving, first, Poisson's equation, and subsequently, the diffusion equation. The specific case we consider is cation migration occurring by two related mechanisms, by isolated cation vacancies and by defect associates of cation and anion vacancies; the electric potential within the space-charge layers shifts the association equilibrium so that associate diffusion dominates in the bulk whereas isolated vacancy diffusion dominates within the space-charge layers. The conditions under which $r > 1$ is observed are described, and issues with experimental confirmation are discussed.

1 Introduction

In ionic solids, grain boundaries, as two-dimensional defects, are not required in electrochemical equilibrium to be locally neutral. Grain boundaries are expected to be electrostatically charged and thus enveloped in compensating space-charge layers to fulfil global electron neutrality. A neutral grain boundary is expected to be the exception. Within the space-charge layers, the concentrations of charged point defects may differ by orders of magnitude from their bulk values, with consequences for those processes that depend directly on defects, such as the transport of ions.

Prime examples of ionic solids with charged grain boundaries are acceptor-doped and acceptor-substituted titanate perovskites. The transport of oxide ions across pristine grain boundaries (i.e. those free of second phases) is known to be hindered.^{1–7} This is attributed to the grain boundaries being positively charged, which leads to the positively charged oxygen vacancies (the defects responsible for oxygen diffusion in these materials) being depleted in the neighboring space-charge layer.^{5,8–12}

Much less attention, however, has been devoted to how space-charge layers affect mass transport along grain boundaries in

these materials. The species that are expected to diffuse at faster rates along space-charge layers than in the bulk phase are cations, since the defects responsible for cation diffusion in perovskites are negatively charged cation vacancies, and these defects will be strongly accumulated in the space-charge layers.^{9,13,14}

Experimentally, faster diffusion of cations along grain boundaries in acceptor-doped perovskite oxides has indeed been observed,^{15–24} but altered point-defect concentrations in space-charge layers are rarely invoked as an explanation. Generally, the observed behaviour is attributed, as in metals, to the atomic arrangement within the grain-boundary core being more open than in the bulk. As in metals, the activation enthalpy of grain-boundary diffusion is expected, therefore, to be roughly half as high as that of bulk diffusion, that is, $r = \Delta H^{gb}/\Delta H^b \approx 0.5$, and thus diffusion, being exponentially dependent on the activation enthalpy, is much faster along grain boundaries than in the bulk, $D^{gb} \gg D^b$. There is a problem, however, in applying this standard picture of faster grain-boundary diffusion to the diffusion of cations in acceptor-doped perovskite oxides. If one examines values of r obtained experimentally (see Fig. 1), one generally finds values well above the $r \approx 0.5$ expected for metals, and in fact, values closer to, and even exceeding, 1. Such values are physically inconsistent with the standard picture, and thus suggest that there is a phenomenon in oxides, but not in metals, that generates $D^{gb} \gg D^b$. The one key difference between met-

^a Institute of Physical Chemistry, RWTH Aachen University, Landoltweg 2, 52074 Aachen, Germany. Fax: +49 241 80 92128; Tel: +49 241 80 94739; E-mail: desouza@pc.rwth-aachen.de, kielgas@pc.rwth-aachen.de

als and oxides, as pointed out by Kingery,²⁵ is that the latter are composed of ions, and as a consequence, space-charge zones may develop at extended defects.

Starting from a thermodynamic description of space-charge layer formation,^{8,10,26} Parras and De Souza used continuum simulations to examine values of r for the case of faster diffusion along space-charge layers at a grain boundary (but not within the core). Their results indicated $r \leq 1$, and they presented quantitative arguments that ruled out higher values of r within their model (of a dilute solution of point defects and diffusion occurring by a single migration mechanism).¹⁵ The question thus arises whether $r > 1$ is due to experimental error or whether, within a different model, it is physically reasonable.

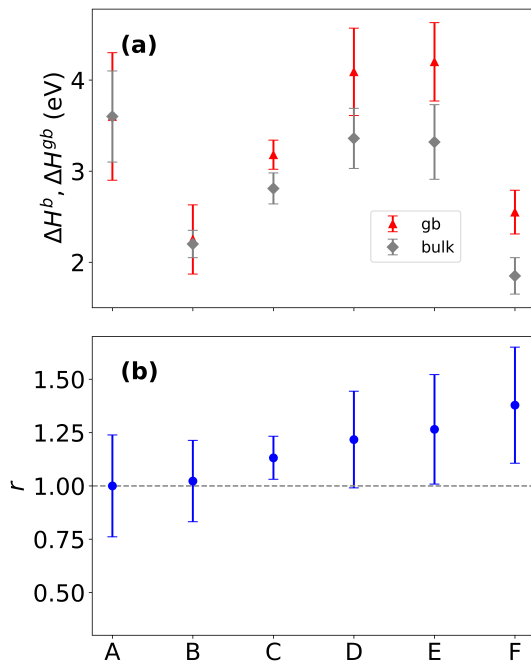


Fig. 1 Cation diffusion in selected ABO_3 perovskite oxides: (a) Activation enthalpies for bulk diffusion ΔH^b and for the grain-boundary diffusion product ΔH^{gb} . (b) The ratio of the activation enthalpies, $r = \Delta H^{gb}/\Delta H^b$. A: Ce in BaZrO₃,²⁷ B: ⁵²Cr in La_{0.8}Sr_{0.2}Ga_{0.8}Mg_{0.2}O_{2.8},²⁸ C: ⁵⁶Fe in LaGaO₃,²⁸ D: Fe-Co interdiffusion in La_{0.6}Sr_{0.4}CoO_{3-δ},²⁴ E: ⁸⁶Sr in La_{0.6}Sr_{0.4}CoO_{3-δ},²⁴ F: ⁵⁶Fe in La_{0.8}Sr_{0.2}Ga_{0.8}Mg_{0.2}O_{2.8},²⁸

In this study, we used continuum simulations to examine if $r > 1$ is physically possible for faster cation diffusion along grain boundaries in perovskite oxides. Specifically, we relax to a limited degree the constraint (used by Parras and De Souza¹⁵) that the migration mechanism is the same in the bulk and in the space-charge layers. The possibility of two completely different migration mechanisms (e.g. vacancy migration in the bulk and interstitial migration in the space-charge layers) is ignored because it is not applicable to cation diffusion in perovskites (Frenkel disorder having prohibitively high formation energies²⁹⁻³⁴) and because it is a somewhat trivial case. Rather, being aware of two strontium-vacancy migration mechanisms in SrTiO₃ (with different activation enthalpies³⁵⁻³⁷) and being aware that the electrostatic potential in a space-charge layer can shift a point-defect equilibrium involving charged defects, we considered the faster diffusion of

Sr along a grain boundary in SrTiO₃. Specifically, both computational and experimental studies indicate that Sr diffusion in SrTiO₃ can occur by the migration of isolated strontium vacancies (with an activation enthalpy of ca. 4 eV) and by the migration of defect associates consisting of a strontium vacancy and an oxygen vacancy (with an activation enthalpy of ca. 3.4 eV).³⁵⁻³⁷ And the specific point-defect equilibrium is the association of a strontium vacancy and an oxygen vacancy to form a defect pair, and the shift occurs because in the negatively charged space-charge layers at grain boundaries in acceptor-doped SrTiO₃, oxygen vacancies are depleted. Consequently, if the association equilibrium favors the associates in the bulk, oxygen-vacancy depletion will shift the equilibrium to isolated strontium vacancies being dominant in the space-charge layers.

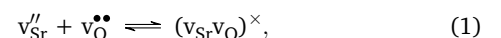
In order to implement this model, we take a similar approach to Parras and De Souza,¹⁵ starting from a thermodynamic description of space-charge formation, using a dilute-solution model of SrTiO₃'s defect chemistry, and focussing on a bicrystal geometry, with the grain boundary situated normal to the surface. We computed point-defect concentrations, and subsequently, Sr cation diffusion profiles in the simulation cell by finite-element-method (FEM) calculations. From these results, we extract the grain-boundary diffusion product $a^{gb}D^{gb}$ and from data as function of temperature, the corresponding activation enthalpy for the grain-boundary diffusion of Sr, ΔH^{gb} , which we then compare to the bulk activation enthalpy ΔH^b .

2 Point-defect concentrations in SrTiO₃

2.1 Bulk-defect Chemistry

The defect chemistry of SrTiO₃ is well established,³⁸⁻⁴⁴ and for the temperatures of interest ($T > 1200$ K), one needs to take the partial Schottky equilibrium for SrO into account (as well as the generation of electron and holes, and the reduction of the oxide). In the present case, this standard defect model needs only to be extended by considering the association of strontium vacancies and oxygen vacancies.

The defect-chemical equilibrium describing the association of strontium vacancies and oxygen vacancies,^{36,37} in Kröger-Vink notation,⁴⁵⁻⁴⁷ reads as

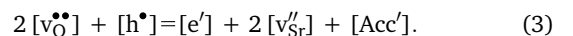


with equilibrium constant

$$K_a = \frac{[(v_{\text{Sr}}v_{\text{O}})^{\times}]}{[v''_{\text{Sr}}] \cdot [v''_{\text{O}}]} = K_a^0 \cdot \exp\left(\frac{\Delta S_a}{k_B}\right) \cdot \exp\left(-\frac{\Delta H_a}{k_B T}\right), \quad (2)$$

where [def] denotes the concentration of species def in m⁻³; K_a^0 is the pre-exponential term; ΔH_a and ΔS_a are the entropy and enthalpy of associate formation.

We consider acceptor-doped SrTiO₃, with an acceptor dopant of constant valence. The electroneutrality condition for this model is thus



The other defect-chemical equilibria are, as mentioned above, the

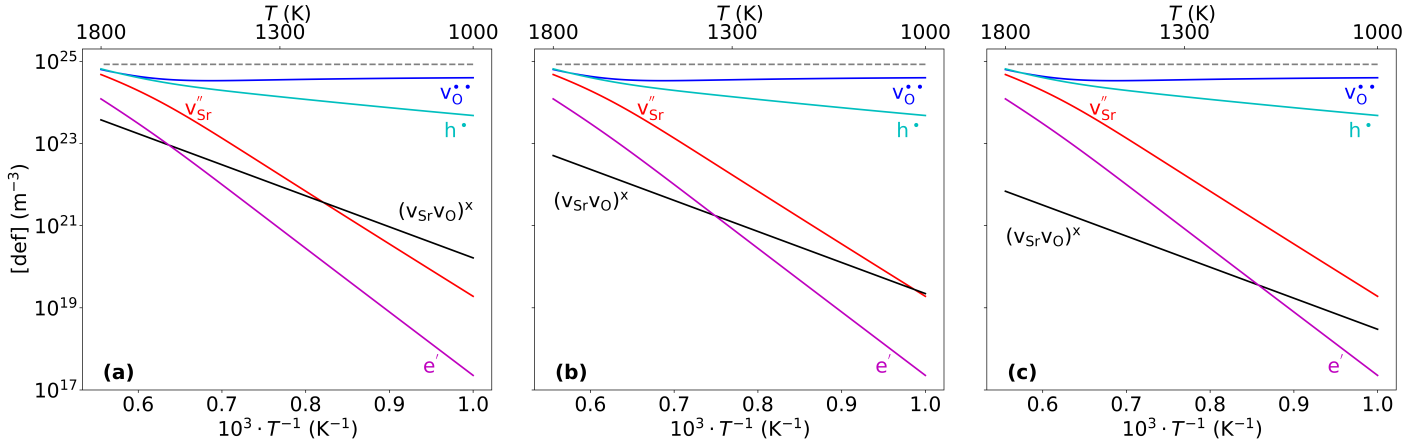


Fig. 2 Bulk concentrations of point defects in acceptor-doped SrTiO_3 as a function of inverse temperature. Gray dashed line indicates $[\text{Acc}']$. Entropy of associate formation is varied: (a) $\Delta S_a = 0 \text{ k}_\text{B}$, (b) $\Delta S_a = -2 \text{ k}_\text{B}$, (c) $\Delta S_a = -4 \text{ k}_\text{B}$. Parameters are $[\text{Acc}'] = 8.43 \cdot 10^{24} \text{ m}^{-3}$, $\Delta H_a = -1 \text{ eV}$, and $a_{\text{O}_2} = 0.2$.

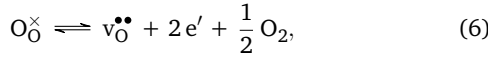
SrO partial-Schottky equilibrium,



with equilibrium constant

$$K_{\text{Sch}} = [v''_\text{Sr}] \cdot [v_\text{O}^{\bullet\bullet}] = K_{\text{Sch}}^0 \cdot \exp\left(-\frac{\Delta H_{\text{Sch}}}{k_\text{B}T}\right); \quad (5)$$

the oxygen reduction reaction,



with equilibrium constant

$$K_{\text{Red}} = [v_\text{O}^{\bullet\bullet}] \cdot [\text{e}']^2 \cdot a_{\text{O}_2}^{0.5} = K_{\text{Red}}^0 \cdot \exp\left(-\frac{\Delta H_{\text{Red}}}{k_\text{B}T}\right); \quad (7)$$

and the thermal excitation of electrons across the band gap to form conduction-band electrons and valence-band holes.



with equilibrium constant

$$K_{\text{eh}} = [\text{e}'] \cdot [\text{h}^{\bullet}] = N_\text{C}(T)N_\text{V}(T) \exp\left(-\frac{E_\text{g}^0 - \beta_\text{g}T}{k_\text{B}T}\right), \quad (9)$$

with the effective density of states in the conduction and valence band $N_\text{C}(T)$, $N_\text{V}(T)$, the band gap E_g^0 , and the temperature coefficient β_g . Values for K_{Sch} , K_{Red} , K_{eh} were calculated from the parameters derived by Moos and Härdtl,⁴⁴ and are listed in Table 1. The association reaction has not been examined experimentally, and hence a value of $\Delta H_a = -1 \text{ eV}$ was used; ΔS_a was taken to have a range of values, $\Delta S_a/k_\text{B} = \{0, -2, -4, -6, -8, -10\}$, in order to shift the temperature at which the association equilibrium is predominantly on the right-hand side or the left-hand side of eqn (1).

Equations [(2), (3), (5), (7), (9)] were solved simultaneously with the Python package Massaction⁴⁸ to yield defect concentrations as a function of temperature for an oxygen activity of $a_{\text{O}_2} = 0.2$. Results are plotted in Fig. 2 for three selected values

Table 1 Parameters used in the defect-chemical model of SrTiO_3 .⁴⁴

Parameter	Value	Unit
K_{Sch}^0	$3 \cdot 10^{56}$	m^{-6}
ΔH_{Sch}	2.5	eV
K_{Red}^0	$5 \cdot 10^{89}$	$\text{m}^{-9} \text{ bar}^{0.5}$
ΔH_{Red}	6.1	eV
$N_\text{C}(T)$	$4.1 \cdot 10^{22} (T/K)^{1.5}$	m^{-3}
$N_\text{V}(T)$	$3.5 \cdot 10^{22} (T/K)^{1.5}$	m^{-3}
E_g^0	3.17	eV
β_g	$5.66 \cdot 10^{-4}$	eV K^{-1}

of ΔS_a . While appreciable cation diffusion in the bulk is not expected for $T < 1200 \text{ K}$,^{37,49,50} it is useful here to consider data below this temperature. Anticipating later results, we make three remarks on the general behaviour shown in Fig. 2. First, the temperature at which the isolated and associated vacancies are equal shifts to lower temperatures with decreasing ΔS_a . Second, $[v''_\text{Sr}]$ remains unaffected by the association equilibrium, even when $[(v_\text{Sr} v_\text{O})^\times] > [v''_\text{Sr}]$ [Fig. (2) (a)], since $[v_\text{O}^{\bullet\bullet}]$ is so high that it fixes $[v''_\text{Sr}]$ through K_{Sch} [eqn (5)]. Third, $[v_\text{O}^{\bullet\bullet}]$ exhibits in all cases a small but clear minimum, and this occurs when $[\text{h}^{\bullet}]$ becomes appreciable relative to $[\text{Acc}']$ and $[v_\text{O}^{\bullet\bullet}]$.

Strontium ions in perovskite SrTiO_3 can, as mentioned above, diffuse by means of isolated as well as by means of associated vacancies,^{35–37} and the respective diffusion coefficients are D_i and D_a . The total diffusivity of strontium cations in the bulk is assumed to be the sum of the two, weighted by their respective site fraction.

$$D_{\text{Sr}} = D_\text{i} \cdot \frac{[v''_\text{Sr}]}{[\text{Sr}_\text{Sr}^\times]} + D_\text{a} \cdot \frac{[(v_\text{Sr} v_\text{O})^\times]}{[\text{Sr}_\text{Sr}^\times]}. \quad (10)$$

Each defect diffusion coefficient D_{def} is given by

$$D_{\text{def}} = \frac{Z_{\text{def}}}{6} d_{\text{Sr}}^2 v_{0,\text{def}} \cdot \exp\left(\frac{\Delta S_{\text{mig,def}}^\ddagger}{k_\text{B}}\right) \cdot \exp\left(-\frac{\Delta H_{\text{mig,def}}^\ddagger}{k_\text{B}T}\right). \quad (11)$$

Z_{def} is the number of jump neighbors ($Z_\text{i} = 6$, $Z_\text{a} = 2$), $d_{\text{Sr}} = 3.905 \cdot 10^{-10} \text{ m}$ the jump distance and v_0 is a characteristic lat-

tice frequency ($v_{0,i} = 10.2 \cdot 10^{12}$ Hz, $v_{0,a} = 20.3 \cdot 10^{12}$ Hz). Values for the migration enthalpies and entropies are taken from meta-dynamic simulations:³⁶ $\Delta H_{\text{mig},i}^{\ddagger} = 3.96$ eV, $\Delta H_{\text{mig},a}^{\ddagger} = 3.41$ eV, $\Delta S_{\text{mig},i}^{\ddagger} = 2.0$ k_B and $\Delta S_{\text{mig},a}^{\ddagger} = 0.88$ k_B .

Eqns (10) and (11) were then used, together with the calculated defect concentrations, to obtain $D_{\text{Sr}}^b(T)$ for different entropies of associate formation. The results are shown in Fig. 3 (a). D_{Sr}^b for different ΔS_a converge at higher temperatures, since isolated v''_{Sr} dominates over associates (cf. Fig. 2). At lower temperatures, D_{Sr}^b is larger for smaller values of ΔS_a , since this yields higher concentrations of the more mobile ($v_{\text{Sr}}v_O$)[×] associate.

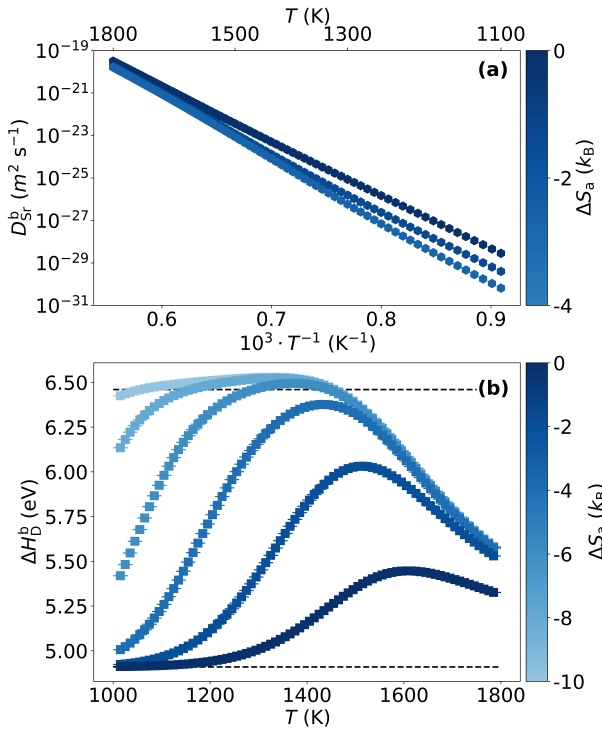


Fig. 3 Bulk diffusion coefficients of strontium in SrTiO_3 calculated from defect concentrations and defect diffusivities for diffusion by means of isolated vacancies and defect associates. (a) Bulk diffusion coefficients as a function of inverse temperature. (b) Activation enthalpy of bulk diffusion over a rolling interval of 40 K, plotted as a function of temperature. Different datasets refer to differing values of the entropy of defect association ΔS_a .

From the $D_{\text{Sr}}^b(T)$ data, the activation enthalpy of strontium diffusion in the bulk is calculated for a rolling average of 40 K [Fig. 3 (b)]. For all values of ΔS_a considered, ΔH_D^b goes through a maximum. This behaviour can, of course, be understood in terms of the defect chemistry and the defect diffusivities. For lower temperatures, the electroneutrality condition can be approximated by $[\text{Acc}'] = 2[v_O^{\bullet\bullet}]$. If the associates provide the dominant contribution to D_{Sr}^b , then the activation enthalpy of strontium diffusion can be shown to be $\Delta H_D^b = \Delta H_{\text{mig},a}^{\ddagger} + \Delta H_a + \Delta H_{\text{Sch}} = 4.91$ eV. For intermediate temperatures, with a dominant contribution from isolated strontium vacancies, and with the same electroneutrality condition, one obtains $\Delta H_D^b = \Delta H_{\text{mig},i}^{\ddagger} + \Delta H_{\text{Sch}} = 6.46$ eV. These values are indicated by dashed lines in Fig. 3. The higher limit is exceeded slightly by the actual data for datasets

with higher ΔS_a because the contribution of the associates to D_{Sr}^b is not negligible. And finally, at the highest temperatures considered, the charge neutrality condition effectively becomes $2[v''_{\text{Sr}}] + [\text{Acc}'] = 2[v_O^{\bullet\bullet}] + [h^{\bullet}]$, and ΔH_D^b decreases.

Since experimental studies of cation diffusion in perovskites are extremely difficult to carry out, and the density of experimental data points as a function of temperature is accordingly rather low, possible deviations from linear Arrhenius behaviour may rarely be directly evident.

2.2 Point-defect concentrations in space-charge layers

We assume that the grain boundary is flat and laterally homogeneous, so that a one-dimensional treatment of the electric potential (in the direction y normal to the grain boundary) is sufficient. We also assume that space-charge formation is driven by the preferential formation of oxygen vacancies in the grain-boundary core,⁸ that is, the standard chemical potential of oxygen vacancies is lower in the grain-boundary core than in the bulk, $\Delta\mu_v^{\circ} = \mu_v^{\circ,c} - \mu_v^{\circ,b} < 0$; $\Delta\mu_{\text{def}}^{\circ}$ is thus set to zero for all other defects. Furthermore, we assume that electrochemical potentials μ_{def} can be defined for point defects in the bulk and in the grain-boundary core, and that they take a (modified) Fermi-Dirac form (see below). And we assume that in electrochemical equilibrium, the electrochemical potentials of mobile defects are constant throughout the system.

It follows that the Poisson equation to be solved [cf. eqn (3)] is

$$-\epsilon_0\epsilon_r \frac{d^2\phi}{dy^2} = e \cdot (-[\text{Acc}'] + 2[v_O^{\bullet\bullet}] - 2[v''_{\text{Sr}}] - [e'] + [h^{\bullet}]), \quad (12)$$

where ϕ is the electric potential and $\epsilon_0\epsilon_r$ is the dielectric permittivity of SrTiO_3 .⁵¹ The boundary conditions are $\nabla\phi^b = 0$ and $\phi^b = 0$. All five (charged) defects are assumed to be sufficiently mobile to achieve electrochemical equilibrium. To obtain the relationship between local concentration and electrostatic potential, we assume, as noted above, electrochemical equilibrium and a modified Fermi-Dirac form of the electrochemical potential of a defect. The modification is required to take account of various species sharing the same sublattice. For the Sr sublattice, for example, Acc' , v''_{Sr} and $(v_{\text{Sr}}v_O)^{\times}$ need to be taken into account. This leads, for instance, to the electrochemical potential of strontium vacancies being

$$\tilde{\mu}_{v''_{\text{Sr}}}(y) = \mu_{v''_{\text{Sr}}}^{\circ} + k_B T \cdot \ln \left(\frac{[v''_{\text{Sr}}](y)}{N_{\text{Sr}} - [v''_{\text{Sr}}](y) - [(v_{\text{Sr}}v_O)^{\times}](y)} \right) + z_{v''_{\text{Sr}}} e\phi(y). \quad (13)$$

Here, N_{Sr} is the site density of the Sr sublattice, $z_{v''_{\text{Sr}}} = -2$ is the charge of a strontium vacancy. Rearrangement of eqn (13) yields

$$[v''_{\text{Sr}}](y) = \frac{N_{\text{Sr}} \cdot [v''_{\text{Sr}}]^b \cdot \exp\left(\frac{+2e\phi(y)}{k_B T}\right)}{N_{\text{Sr}}^b + [v''_{\text{Sr}}]^b \cdot \exp\left(\frac{+2e\phi(y)}{k_B T}\right) - [v''_{\text{Sr}}]^b} \quad (14)$$

The equivalent expression for the concentration of oxygen vacancies, including the thermodynamic driving energy for space-

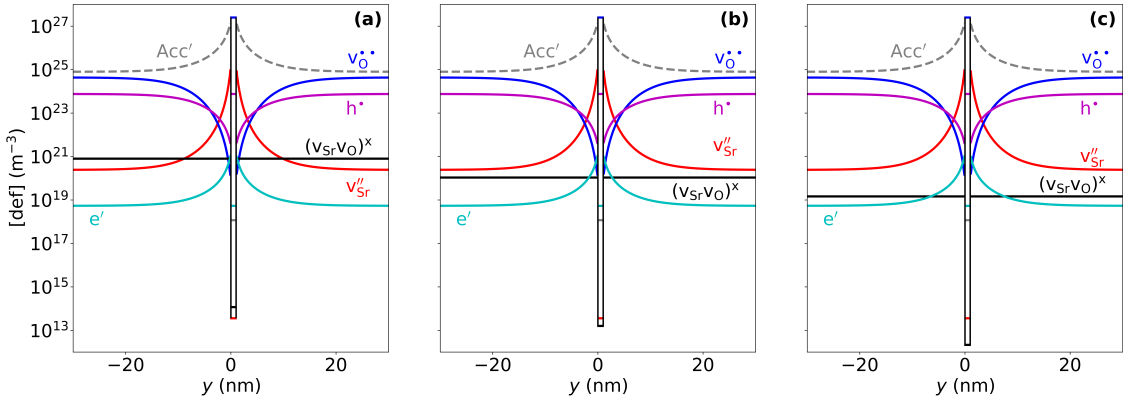


Fig. 4 Calculated defect concentrations normal to a grain boundary. Entropy of associate formation is varied: (a) $\Delta S_a = 0 \text{ k}_B$, (b) $\Delta S_a = -2 \text{ k}_B$, (c) $\Delta S_a = -4 \text{ k}_B$. Simulation parameters: $T = 1100 \text{ K}$, $\Delta S_a = -2 \text{ k}_B$ [$\text{Acc}' = 8.43 \cdot 10^{24} \text{ m}^{-3}$]. GB-core ($0 \text{ nm} < y < 1 \text{ nm}$) calculated with $\Delta \mu_v^\diamond = -2 \text{ eV}$.

charge formation $\Delta \mu_v^\diamond$ reads

$$[\text{v}_O^{\bullet\bullet}]^b(y) = \frac{[\text{v}_O^{\bullet\bullet}]^b \cdot \exp\left(\frac{-2e\phi(y) - \Delta \mu_v^\diamond}{k_B T}\right) \cdot (N_0 - [(v_{\text{Sr}} v_{\text{O}})^x](y))}{N_0^b - [(v_{\text{Sr}} v_{\text{O}})^x]^b + [\text{v}_O^{\bullet\bullet}]^b \cdot \exp\left(\frac{-2e\phi(y) - \Delta \mu_v^\diamond}{k_B T}\right) - [\text{v}_O^{\bullet\bullet}]^b} \quad (15)$$

Expressions for electron and hole concentrations follow the standard Maxwell–Boltzmann form $c_{\text{def}} = c_{\text{def}}^b \exp(z_{\text{def}} e\phi(y)/k_B T)$.⁹

The spatial variation in the concentration of the associates does not enter the Poisson equation, since the species are neutral. The variation is required, however, to calculate local strontium diffusivity according to eqn (10). The expression for the associates reads

$$[(v_{\text{Sr}} v_{\text{O}})^x](y) = \frac{[v''_{\text{Sr}}](y)}{[v''_{\text{Sr}}]^b \cdot \exp\left(\frac{2e\phi(y)}{k_B T}\right)} \quad (16)$$

Defect concentrations as a function of distance from the grain boundary core are illustrated in Fig. 4 for given T and a_{O_2} and different ΔS_a . Oxygen vacancies are depleted, acceptor-dopant cations and isolated strontium vacancies are accumulated in the space-charge layer. Since the acceptor-dopants have a significantly higher concentration than isolated strontium vacancies in the space-charge layer, it is their behaviour that governs the extent of the space-charge layer and the degree to which charged mobile defects are accumulated or depleted. The concentration of associates shows no significant change close to the space-charge layer, due to its neutral charge and the depletion of oxygen vacancies, needed to form associates.

3 Obtaining the Grain-Boundary Diffusion Product

To investigate strontium cation diffusion along the space-charge layers at a grain boundary, we consider a two-dimensional cell consisting of two SrTiO_3 grains, sandwiching the grain-boundary core. Cations may diffuse into the cell from an infinite source on one side normal to the grain boundary, as shown in Fig. 5 (a).

The simulation is executed in three steps. First, bulk concen-

trations of defects in thermodynamic equilibrium are calculated (Sec. 2.1). Then, the local electrostatic potential (and local defect concentrations) are obtained by solving Poisson's equation (Sec. 2.2). Third, the diffusion equation,

$$\frac{\partial [\text{Sr}](x, y)}{\partial t} = \nabla \cdot \{D_{\text{Sr}}(y) \nabla [\text{Sr}](x, y)\}, \quad (17)$$

is solved for the strontium tracer cations for a diffusion time t_D . Since we require diffusion within the core to be negligible compared with diffusion within the space-charge layers at the grain boundary, so that the latter dominates the behaviour, the cation diffusivity within the core is set to $D_{\text{Sr}}^c = 10^{-6} \cdot D_{\text{Sr}}^b$. For each temperature, a diffusion time t_D was calculated, so that a constant bulk diffusion length of $l_D = \sqrt{D_{\text{Sr}}^b \cdot t} = 20 \text{ nm}$ was obtained. Steps two and three were carried out by means of finite-element-method (FEM) calculations (COMSOL®Multiphysics®, Ver. 6.1, Stockholm, Sweden). The result of one such set of calculations is a two-dimensional distribution of the Sr tracer cations, as shown in Fig. 5 (b).

From the simulated two-dimensional concentration distribution, a linear projection of the y axis onto the x axis was performed to obtain a one-dimensional depth profile of strontium tracer concentration versus depth from the surface, similar to an experimental depth profile obtained by Secondary Ion Mass Spectrometry (SIMS). The simulation parameters were chosen to produce diffusion profiles referring to Harrison B-type diffusion kinetics⁵² with two distinct features evident (see Fig. 6), corresponding to slow diffusion in the bulk and faster diffusion along the grain boundary and slow bulk diffusion out of it.

Given the chosen initial and boundary conditions, the appropriate solution to the diffusion equation is a complementary error function,⁵³ and unsurprisingly this mathematical form describes the first feature well, as shown in Fig. 6 (a), to yield D_{Sr}^b . Values obtained in this manner are very close to the D_{Sr}^b values used as input [taken from Fig. 3 (a)], with deviations being less than 3 %.

The grain-boundary feature exhibits linear behaviour in a plot of $\ln[\text{Sr}]$ versus $\eta^{6/5}$ [Fig. 6 (b)], where $\eta = y/\sqrt{D_{\text{Sr}}^b t_D}$, as expected for faster grain-boundary diffusion. The slope of this second feature was analysed according to the method proposed by Chung and Wuensch,⁵⁴ which takes the slope between $6 \leq \eta \leq 10$. The

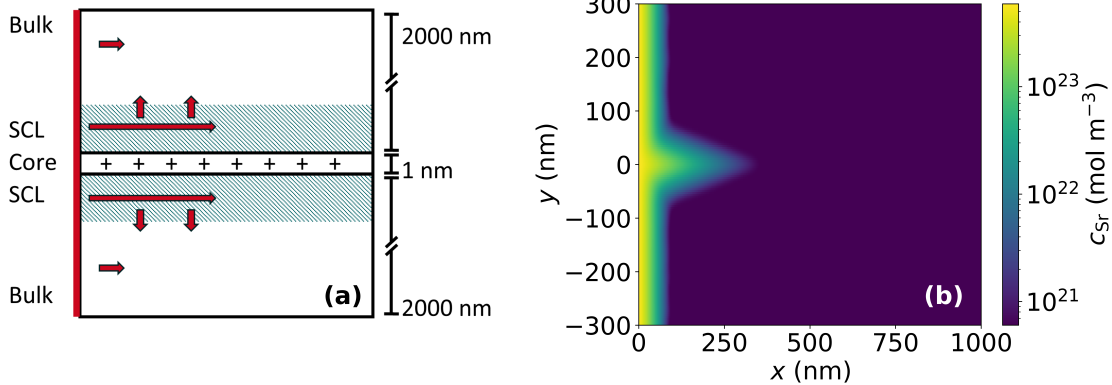


Fig. 5 (a) Two-dimensional simulation cell of two grains separated by a grain boundary. The grain boundary consist of an interface core and adjacent space charge layer. Ions come from an undepletable source on the left side and diffuse via the red arrows, into the bulk, along the SCL and from the SCL into the bulk. (b) Concentration profile of strontium ions after finished simulation, with enhanced diffusion along the grain boundary.

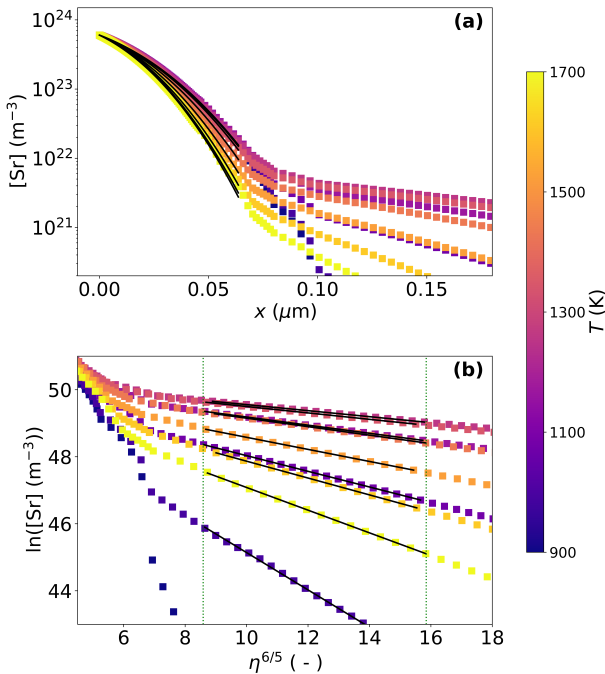


Fig. 6 Strontium tracer diffusion profiles at different temperatures, for the bicrystal geometry of Fig. 5 (a). Diffusion times were chosen so that the bulk diffusion length was the same for all temperatures. (a) strontium tracer concentration versus depth, together with an error function fit to the bulk feature, (b) concentration as a function of $\eta^{6/5}$, with linear fit to the grain-boundary 'tail'. Simulation parameters: $\Delta S_a = -2 \text{ k}_B$ $[\text{Acc}'] = 8.43 \cdot 10^{-24} \text{ m}^{-3}$, $\Delta H_a = -1 \text{ eV}$, $\Delta \mu_v^\circ = 2 \text{ eV}$, $N_{\text{V}_0}^{\text{gb}} = 2.5 \cdot 10^{27} \text{ m}^{-3}$, $N_{\text{V}_{\text{Sr}}}^{\text{gb}} = N_{\text{V}_0}^{\text{gb}} \cdot 10^{-6}$.

grain-boundary diffusion product $a^{\text{gb}}D_{\text{Sr}}^{\text{gb}}$ is then obtained according to

$$a^{\text{gb}}D_{\text{Sr}}^{\text{gb}} = (D^b)^{3/2} \cdot t^{1/2} \left[10^A \left(-\frac{\partial \ln[\text{Sr}]}{\partial \eta^{6/5}} \right)^B \right]. \quad (18)$$

Values of A and B were derived by Chung and Wuensch.⁵⁴ In order to get diffusion profiles with a sufficient grain-boundary feature for analysis, we only consider data for which $\beta \geq 10$, with

$\beta = a^{\text{gb}}D_{\text{Sr}}^{\text{gb}} / ((D^b)^{3/2} \cdot t^{1/2})$, representing a ratio of grain-boundary to bulk diffusion.

4 Results and Discussion

The grain-boundary diffusion products obtained from the simulations for a range of temperatures are plotted in Fig. 7 (a) for selected values of ΔS_a . The data all fall together on a single line; data for lower ΔS_a (not shown) also fall on this line. For the same selected ΔS_a , the bulk diffusivities of Sr do vary [Fig. 7 (d) reproduced from Fig. 3(a)]. The reason for this difference is that D_{Sr}^b has contributions from associated and isolated strontium vacancies, whereas $a^{\text{gb}}D_{\text{Sr}}^{\text{gb}}$ refers primarily to isolated strontium vacancies, as these are the defects that are strongly accumulated in the space-charge layers.

Since space-charge layers are regions of modified bulk defect chemistry, one can understand the observed behaviour in terms of (i) the relevant bulk defect concentrations and (ii) the degree of their modification in the space-charge layers. Thus, we first show in Fig. 7 (b) the contribution of the Sr diffusivity arising solely from isolated strontium vacancies, that is $D_{\text{Sr}}^b[\text{V}_{\text{Sr}}^{\text{gb}}]/[\text{Sr}_{\text{Sr}}^{\text{gb}}]$, see (10); and since, as noted previously, $[\text{V}_{\text{Sr}}^{\text{gb}}]^b$ is unaffected by the association equilibrium, we find that $D_{\text{Sr},i}^b$ is also independent of ΔS_a . In Fig. 7 (c) we show the space-charge potential Φ_0 , and in this case, as also noted previously, since the accumulation of the acceptor-dopant cations, $[\text{Acc}'](\text{y})$, governs the screening within the space-charge layers, the space-charge potential is also independent of ΔS_a . In this way, we understand why all the $a^{\text{gb}}D_{\text{Sr}}^{\text{gb}}$ fall together and are independent of ΔS_a . We also understand that the relevant bulk defect concentration is $[\text{V}_{\text{Sr}}^{\text{gb}}]$, since it is these defects whose concentration is enhanced in the space-charge layers, giving rise to faster diffusion along the grain boundary.

This understanding can also be placed on a quantitative level. Parras and De Souza¹⁵ derived an approximate expression for the grain-boundary diffusion product (in the case of diffusion along space-charge layers) in terms of the bulk diffusion coefficient, the Debye length ℓ_D and the space-charge potential,

$$a^{gb} D_{pred,i}^{gb}(T) = 2\ell_D(T) f_\ell \cdot D_{Sr,i}^b(T) \cdot \exp\left(-\frac{f_P z_{v_{Sr}} e \cdot \Phi_0(T)}{k_B T}\right), \quad (19)$$

with the parameters $f_\ell = 0.205$ and $f_P = 0.854$. The Debye length, $\ell_D = \sqrt{\epsilon_0 \epsilon_r k_B T / (2e^2 [Acc]^b)}$, is weakly dependent on temperature in the present case, not only through the explicit presence of T but also through the Curie–Weiss behaviour of ϵ_r in SrTiO_3 ⁵¹.

Eqn (19) essentially expresses the fact that faster grain-boundary diffusion along space-charge layers can be considered to be accelerated (i) over a distance a^{gb} , which is some fraction f_ℓ of twice the Debye length, and (ii) by an amount given by the exponential term, which refers to an effective average (hence: f_P) over the entire space-charge layer. With the data in Fig. 7 (b) and (c) we thus calculated $a^{gb} D_{pred,i}^{gb}$, and we compare the values in Fig. 7 (a). We find good agreement between the values from the simulations and the values predicted with (19), the difference being less than a factor of 3. In this way the main points from above are confirmed quantitatively.

Now we come to the main question of this study, and the possibility of $r > 1$. In Fig. 8 (a) we plot the activation enthalpy of the grain boundary diffusion product obtained for a rolling interval of 40 K. $\Delta H_D^b(T)$ decreases monotonically with increasing temperature, and is not a function of ΔS_a , reflecting the behaviour of Fig. 7 (a). In contrast, ΔH_D^b [Fig. 3 (b)] tends to go through a maximum with increasing temperature and is a function of ΔS_a .

Combining the data of Fig. 8 (a) and Fig. 3 (b) we obtain r as a function of temperature for various values of ΔS_a [Fig. 8 (b)]. The datasets for the most negative values of ΔS_a correspond essentially to the case of isolated strontium vacancies being present in higher concentrations than the associates in the bulk. These data show $r < 1$. The datasets for the higher values of ΔS_a refer to a strong contribution to $D_{Sr,i}^b$ from $(v_{Sr}v_O)^\times$ associates, especially at lower temperatures, and it is under these conditions that we find $r > 1$. For $\Delta S_a/k_B = -2$, for instance, r attains values up to 1.15 for the temperature range considered. Beyond the fact that $r > 1$ is possible, we emphasise the fact that r varies with temperature.

The behaviour of r in Fig. 8 (b) suggests that even higher values of r may be attained at even lower temperatures, and thus it raises the question of whether there is a limit to r for this model. For the case of a single diffusion mechanism,¹⁵ $r \leq 1$ was established as the physical limit based on the behaviour of $\Phi_0(T)$. In the present case, we can extend the arguments of Parra and De Souza¹⁵ to the more complicated model. The first part is that the highest possible value of ΔH_D^{gb} is $\Delta H_{D,i}^b \approx 6.5$ eV (i.e. that of the isolated strontium vacancies), and it corresponds to $r = 1$ for the isolated vacancies. The second part is that $r > 1$ is generated by ΔH_D^b being lower than $\Delta H_{D,i}^b$ through a dominant contribution from the $(v_{Sr}v_O)^\times$ associates. And the lowest value for ΔH_D^b is 4.9 eV. Thus, putting the two parts together we obtain — for this system, with these defect chemical parameters — an upper limit of $r \leq 1.3$.

5 Concluding Remarks

Using an established set of defect chemical parameters for the bulk of acceptor-doped SrTiO_3 ; using physically reasonable val-

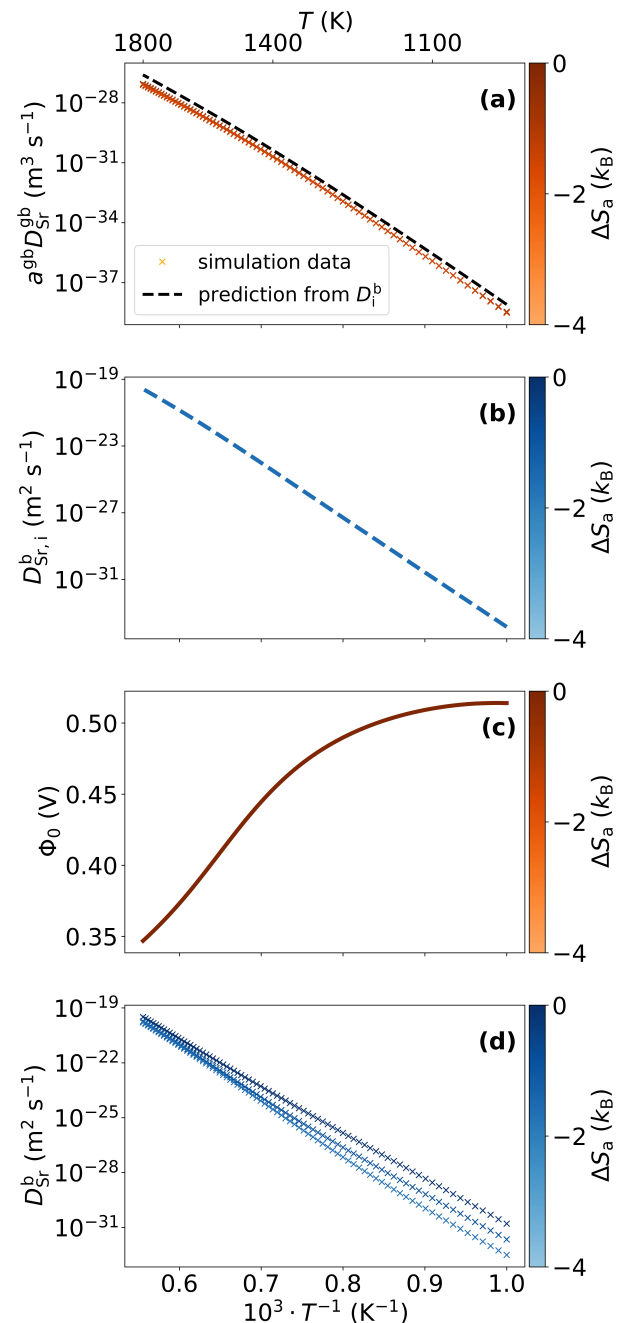


Fig. 7 Simulation properties for bulk and grain-boundary as function of inverse temperature. (a) grain-boundary diffusion product $a^{gb} D_{Sr,i}^{gb}$, and predicted $a^{gb} D_{pred,i}^{gb}$ from eqn (19). (b) bulk diffusion coefficient $D_{Sr,i}^b$ arising solely from the diffusion of isolated strontium vacancies. (c) space-charge potential Φ_0 . (d) bulk diffusion coefficient $D_{Sr,i}^b$ from error function fit. Note that for all but (d) Data for different ΔS_a are plotted but overlay each other.

ues of ΔS_a and ΔH_a for the formation of $(v_{Sr}v_O)^\times$ associates; using defect diffusivities that show higher values for the associate than for the isolated vacancy; using a standard thermodynamic model of space-charge formation; and taking a reasonable value for the thermodynamic driving energy of space-charge formation $\Delta \mu_v^\phi$; we find for the faster diffusion of cations along the space-charge layers at a grain boundary ($D^{\text{text}}_{gb} > D^b$) that $r > 1$ is indeed pos-

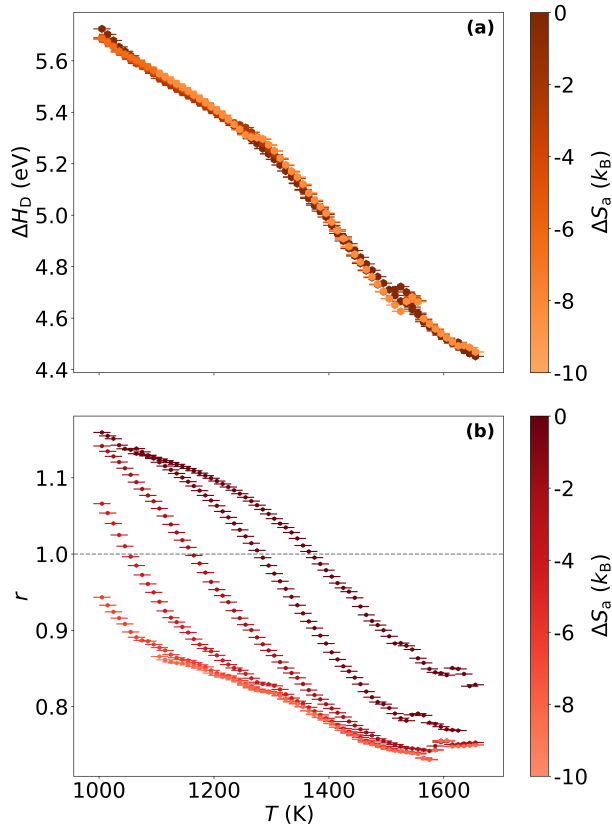


Fig. 8 (a) temperature dependent activation enthalpies of strontium cation grain-boundary diffusion over rolling intervals of 40 K for different entropy of associate formation. (b) ratio r of activation enthalpies of diffusion in the grain boundary and the bulk as a function of temperature, with varied Entropy of associate formation. Unity of r is indicated by a gray dashed line.

sible.

To test this model, experimental studies are necessary for comparison. And in performing such studies, the range of temperatures considered is extremely important: as we have found, r is a function of temperature and tends to exceed unity at lower rather than higher temperatures. Common temperature ranges for experimental cation diffusion studies in titanate perovskites are in the range $1200 \leq T/K \leq 1500$.^{37,49,50,55,56} In this temperature range, our simulation for $\Delta S_a/k_B = -2$ predicts $r > 1$. But in our simulations we have a high density of data points, and this will generally not be the case in experiment. Indeed, if one only considers five data points, $T/K = \{1200, 1250, 1300, 1350, 1400\}$, one would obtain $\Delta H_D^{gb} = (5.22 \pm 0.04)$ eV and $\Delta H_D^b = (5.31 \pm 0.05)$ eV, hence a ratio of $r = 0.98 \pm 0.01$ (for $\Delta S_a/k_B = -2$). Thus, an even lower temperature range is necessary for an experimental study to be able to demonstrate $r > 1$. For five temperatures in the range $1100 \leq T/K \leq 1300$, we predict $\Delta H_D^{gb} = (5.42 \pm 0.03)$ eV and $\Delta H_D^b = (5.08 \pm 0.03)$ eV, and hence $r = 1.07 \pm 0.01$.

Finally, we comment on the applicability of this model to other systems. We presume that the general behaviour is applicable to the diffusion of A cations in all ABO_3 perovskites, first because the formation of (v_{AV_O}) associates is highly likely given the opposite relative charges of the two constituent defects, and second, be-

cause the higher diffusivity of the associate is expected as a characteristic of the ABO_3 perovskite structure. Indeed, for $BaTiO_3$, $(v_{Ba}v_O)$ associates are predicted to be bound,⁵⁷ and they have recently been predicted⁵⁸ to have higher diffusivities than isolated v''_{Ba} . That said, (v_{AV_O}) associates are not the only associates containing cation vacancies that may form in a perovskite, and the presence of significant concentrations of (v_{AV_O}) associates^{58,59} or $(v_{AV}v_O)$ clusters^{60,61} may give rise to even richer cation diffusion behaviour.

Acknowledgements

This study has received funding from the Deutsche Forschungsgemeinschaft (DFG, German Research Foundation) within project 463184206 (SFB 1548, FLAIR: Fermi Level Engineering Applied to Oxide Electroceramics). Discussions with Matthew J. Wolf are acknowledged.

Notes and references

- 1 C. Schaffrin, *Phys. Stat. Sol. (a)*, 1976, **35**, 79–88.
- 2 K. Watanabe, I. Sakaguchi, S. Hishita, H. Haneda and N. Ohashi, *Key Eng. Mater.*, 2013, **566**, 262–265.
- 3 M. Leonhardt, *Electrochem. Solid-State Lett.*, 1999, **2**, 333.
- 4 R. Waser, *J. Am. Ceram. Soc.*, 1989, **72**, 2234–2240.
- 5 I. Denk, F. Noll and J. Maier, *J. Am. Ceram. Soc.*, 1997, **80**, 279–285.
- 6 R. A. De Souza, J. Fleig, J. Maier, O. Kienzle, Z. Zhang, W. Sigle and M. Rühle, *J. Am. Ceram. Soc.*, 2003, **86**, 922–928.
- 7 R. A. De Souza, C. Voisin, H. Schraknepper, M. Teusner, M. Kessel, P. Dufour, C. Tenailleau and S. Guillemet-Fritsch, *Phys. Chem. Chem. Phys.*, 2014, **16**, 2568–2575.
- 8 R. A. De Souza, *Phys. Chem. Chem. Phys.*, 2009, **11**, 9939–9969.
- 9 A. L. Usler, F. Ketter and R. A. De Souza, *Phys. Chem. Chem. Phys.*, 2024, **26**, 8287–8298.
- 10 P. C. McIntyre, *J. Am. Ceram. Soc.*, 2000, **83**, 1129–1136.
- 11 R. Waser, *Solid State Ionics*, 1995, **75**, 89–99.
- 12 R. Waser and R. Hagenbeck, *Acta Mater.*, 2000, **48**, 797–825.
- 13 A. L. Usler and R. A. De Souza, *J. Electrochem. Soc.*, 2021, **168**, 056504.
- 14 G. Garcia-Belmonte and O. Almora, *APL Energy*, 2025, **3**, 036103.
- 15 J. P. Parras and R. A. De Souza, *Acta Mater.*, 2020, **195**, 383–391.
- 16 I. Wærnhus, N. Sakai, H. Yokokawa, T. Grande, M.-A. Einarsrud and K. Wiik, *Solid State Ionics*, 2007, **178**, 907–914.
- 17 R. Sažinas, I. Sakaguchi, I. Hasle, J. M. Polfus, R. Haugsrud, M.-A. Einarsrud and T. Grande, *Phys. Chem. Chem. Phys.*, 2017, **19**, 21878–21886.
- 18 R. Sažinas, I. Sakaguchi, M.-A. Einarsrud and T. Grande, *AIP Adv.*, 2017, **7**, 115024.
- 19 M. Palcut, J. S. Christensen, K. Wiik and T. Grande, *Phys. Chem. Chem. Phys.*, 2008, **10**, 6544–6552.
- 20 D. Yamazaki, T. Kato, H. Yurimoto, E. Ohtani and M. Toriumi,

Phys. Earth Planet. Inter., 2000, **119**, 299–309.

21 J. Itoh, H. Haneda, S. Hishita, I. Sakaguchi, N. Ohashi, D.-C. Park and I. Yashima, *J. Mater. Res.*, 2004, **19**, 3512–3520.

22 J. B. Smith, T. Norby and A. Fosdal, *J. Am. Ceram. Soc.*, 2006, **89**, 582–586.

23 S. P. Harvey, R. A. De Souza and M. Martin, *Energy Environ. Sci.*, 2012, **5**, 5803–5813.

24 M. Kubicek, G. M. Rupp, S. Huber, A. Penn, A. K. Opitz, J. Bernardi, M. Stöger-Pollach, H. Hutter and J. Fleig, *Phys. Chem. Chem. Phys.*, 2014, **16**, 2715–2726.

25 W. D. Kingery, *J. Am. Ceram. Soc.*, 1974, **57**, 74–83.

26 A. Tschöpe, *Solid State Ionics*, 2001, **139**, 267–280.

27 I. Hasle, S. P. Waldow, U. N. Gries, R. A. De Souza, E. Vøllestad and R. Haugsrud, *J. Mater. Chem. A*, 2021, **9**, 21142–21150.

28 O. Schulz, 2003 (in German).

29 B. Liu, V. R. Cooper, H. Xu, H. Xiao, Y. Zhang and W. J. Weber, *Phys. Chem. Chem. Phys.*, 2014, **16**, 15590–15596.

30 M. J. Akhtar, Z.-U.-N. Akhtar, R. A. Jackson and C. R. A. Catlow, *J. Am. Ceram. Soc.*, 1995, **78**, 421–428.

31 B. S. Thomas, N. A. Marks and B. D. Begg, *Nucl. Instrum. Methods Phys. Res., Sect. B*, 2007, **254**, 211–218.

32 S. J. Stokes and M. S. Islam, *J. Mater. Chem.*, 2010, **20**, 6258.

33 R. A. De Souza and J. Maier, *Phys. Chem. Chem. Phys.*, 2003, **5**, 740–748.

34 R. A. De Souza, M. S. Islam and E. Ivers-Tiffée, *J. Mater. Chem.*, 1999, **9**, 1621–1627.

35 A. Walsh, C. R. A. Catlow, A. G. H. Smith, A. A. Sokol and S. M. Woodley, *Phys. Rev. B*, 2011, **83**, 220301.

36 H. J. Heelweg and R. A. De Souza, *Phys. Rev. Mater.*, 2021, **5**, 103804.

37 U. N. Gries, M. Kessel, F. V. E. Hensling, R. Dittmann, M. Martin and R. A. De Souza, *Phys. Rev. Mater.*, 2020, **4**, 123404.

38 U. Balachandran and N. G. Eror, *J. Solid State Chem.*, 1981, **39**, 351–359.

39 N. H. Chan, R. K. Sharma and D. M. Smyth, *J. Electrochem. Soc.*, 1981, **128**, 1762–1769.

40 G. M. Choi, H. L. Tuller and D. Goldschmidt, *Phys. Rev. B*, 1986, **34**, 6972–6979.

41 G. M. Choi and H. L. Tuller, *J. Am. Ceram. Soc.*, 1988, **71**, 201–205.

42 R. Waser, *J. Am. Ceram. Soc.*, 1991, **74**, 1934–1940.

43 I. Denk, W. Münch and J. Maier, *J. Am. Ceram. Soc.*, 1995, **78**, 3265–3272.

44 R. Moos and K. H. Hardtl, *J. Am. Ceram. Soc.*, 1997, **80**, 2549–2562.

45 F. A. Kröger and H. J. Vink, *Solid State Physics*, Academic Press, 1956, vol. 3, pp. 307–435.

46 T. Norby, *J. Korean Ceram. Soc.*, 2010, **47**, 19–25.

47 R. De Souza and G. Harrington, *Nat. Mater.*, 2023, **22**, 794–797.

48 A. L. Usler, *massaction*, 2024, <https://www.zenodo.org/>.

49 K. Gömann, G. Borchardt, M. Schulz, A. Gömann, W. Maus-Friedrichs, B. Lesage, O. Kaitasov, S. Hoffmann-Eifert and T. Schneller, *Phys. Chem. Chem. Phys.*, 2005, **7**, 2053–2060.

50 R. Meyer, R. Waser, J. Helmbold and G. Borchardt, *Phys. Rev. Lett.*, 2003, **90**, 105901.

51 J. Maier, G. Schwitzgebel and H.-J. Hagemann, *J. Solid State Chem.*, 1985, **58**, 1–13.

52 L. G. Harrison, *Trans. Faraday Soc.*, 1961, **57**, 1191.

53 J. Crank, *The mathematics of diffusion*, Univ. Pr, 2nd edn, 2011.

54 Y.-C. Chung and B. J. Wuensch, *J. Appl. Phys.*, 1996, **79**, 8323–8329.

55 T. Bak, J. Nowotny and C. C. Sorrel, *J. Phys. Chem. Solids*, 2004, **65**, 1229–1241.

56 S. Koerfer, R. A. De Souza, H.-I. Yoo and M. Martin, *Solid State Sci.*, 2008, **10**, 725–734.

57 P. Erhart and K. Albe, *J. Appl. Phys.*, 2007, **102**, 084111–084118.

58 S. Koerfer, B. Dißmann, N. Schier, H.-I. Yoo, M. Martin and R. A. De Souza, *arXiv*, <https://doi.org/10.48550/arXiv.2601.09344>, 2026, 0.

59 A. Bonkowski, M. J. Wolf, J. Wu, S. C. Parker, A. Klein and R. A. De Souza, *J. Am. Chem. Soc.*, 2024, **146**, 23012–23021.

60 O. Schulz, M. Martin, C. Argirasis and G. Borchardt, *Phys. Chem. Chem. Phys.*, 2003, **5**, 2308–2313.

61 I. V. Belova, G. E. Murch, D. Samuelis and M. Martin, *Defect Diffus. Forum*, 2007, **263**, 81–86.